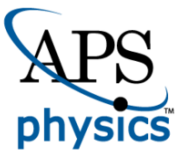

Space-Time Quantum Metasurfaces

Wilton J. M. Kort-Kamp, Abul K. Azad, and Diego A. R. Dalvit

Phys. Rev. Lett. **127**, 043603 — Published 20 July 2021

DOI: 10.1103/PhysRevLett.127.043603

Space-Time Quantum Metasurfaces

Wilton J. M. Kort-Kamp,[1] Abul K. Azad,[1] and Diego A. R. Dalvit*[1]

[1]*Los Alamos National Laboratory, Los Alamos, NM 87545, USA*

(Dated: June 7, 2021)

Metasurfaces have recently entered the realm of quantum photonics, enabling manipulation of quantum light using a compact nanophotonic platform. Realizing the full potential of metasurfaces at the deepest quantum level requires the ability to tune coherent light-matter interactions continuously in space and time. Here, we introduce the concept of space-time quantum metasurfaces for arbitrary control of the spectral, spatial, and spin properties of nonclassical light using a compact photonic platform. We show that space-time quantum metasurfaces allow on-demand tailoring of entanglement among all degrees of freedom of a single photon. We also show that spatio-temporal modulation induces asymmetry at the fundamental level of quantum fluctuations, resulting in the generation of steered and vortex photon pairs out of vacuum. Space-time quantum metasurfaces have the potential to enable novel photonic functionalities, such as encoding quantum information into high-dimensional color qudits using designer modulation protocols, sculpting multispectral and multispatial modes in spontaneous emission, and generating reconfigurable hyperentanglement for high-capacity quantum communications.

The generation, manipulation, and detection of nonclassical states of light is at the heart of quantum photonics. As quantum information can be encoded into the different degrees of freedom of a single photon, it is highly desirable to develop photonic platforms that allow to control them while maintaining quantum coherence. Metasurfaces [1, 2] have recently transitioned from the classical to the quantum domain [3–16]. Demonstrations of metasurfaces in quantum photonics are based on meta-atoms whose optical properties are determined by their material composition and geometrical design, and the lack of spatio-temporal control severely limits the functionalities that state-of-the-art quantum metasurfaces can attain. At the classical level, space-time metasurfaces have been shown to provide that higher degree of control [17, 18], both by reconfigurable and fully-dynamic tailoring of the optical response of meta-atoms using analog and digital modulation schemes [19, 20]. Transitioning spatio-temporal modulation through the classical-quantum divide could be critical to enable novel opportunities for flat quantum photonics.

Here, we put forward the concept of space-time quantum metasurfaces (STQMs) for spatio-temporal control of quantum light. In the STQM paradigm, meta-atoms are modulated in space and time enabling manipulation of quantum light interacting with the dynamical metasurface. STQMs come in different flavors, including modulated quantum systems such as atomic arrays driven by laser pulses, hybrid quantum-classical systems such as quantum emitters embedded in modulated dielectric nanostructures, and meta-atoms made of classical or quantum materials with driven optical or electro-optical response. In this work we discuss concrete examples for the last two flavors. Figure 1a depicts an all-dielectric STQM for generating multicolor-multipath-spin hyperentanglement on a single photon. Figure 1b illustrates a graphene-based STQM generating vortex dynamical Casimir photons out of the quantum vacuum.

STQM-enabled entanglement manipulation: We first study the entanglement dynamics of a single photon as it transits through a dielectric metasurface whose permittivity is spatio-temporally modulated. The meta-atoms are comprised of high-index dielectrics, that have low optical absorption and result in negligible photon loss. The identical meta-atoms are anisotropic and are suitably rotated with respect to each other (Fig. 1a). The combination of anisotropy and rotation results in circular cross-polarization conversion and a spin-dependent Pancharatnam-Berry geometric phase distribution $\Psi(\mathbf{r})$ akin to spin-orbit coupling [21]. The spatio-temporal modulation is modeled as a harmonic perturbation to the permittivity, $\epsilon(\mathbf{r},t) = \epsilon_{um} + \Delta\epsilon\cos(\Omega t - \Phi(\mathbf{r}))$, where ϵ_{um} is the unmodulated permittivity, $\Delta\epsilon$ the modulation amplitude, Ω the modulation frequency, and $\Phi(\mathbf{r})$ a "synthetic" phase. Such kind of modulation has been recently demonstrated in [22] using an amorphous Si optical metasurface and two slightly detuned near-IR pump beams. Their interference produces a traveling-wave permittivity modulation via the nonlinear Kerr effect in amorphous Si, resulting in $\Phi(\mathbf{r}) = \boldsymbol{\beta}\cdot\mathbf{r}$ and with modulation frequency given by the detuning of the pumps [23]. Note that the geometric phase is fixed by the design of the metasurface, while the modulation momentum "kick" $\boldsymbol{\beta}$ can be reconfigured on-demand.

The geometry of the meta-atoms can be tailored so that their lowest Mie electric and magnetic dipolar resonances dominate the optical response and the STQM has maximal cross-polarized transmission [23]. One can then describe the interaction of each resonator with light using the Hamiltonian $H_{int} = -\mathbf{p}\cdot\mathbf{E} - \mathbf{m}\cdot\mathbf{B}$ [32, 33], where $\mathbf{p}$ and $\mathbf{m}$ are the electric and magnetic dipole operators and $\mathbf{E}$ and $\mathbf{B}$ are the quantized electromagnetic fields. It is convenient to express the Hamiltonian only in terms of photonic modes by relating dipoles and fields via effective electric $\boldsymbol{\alpha}_E$ and magnetic $\boldsymbol{\alpha}_M$ polarizability tensors. Cross-polarized transmission of a normally incident photon can be described via an unmodulated coupling strength $\alpha_{um}^{(cr)}(\omega) = \mathrm{Re}[\alpha_{E,xx}(\omega) + \alpha_{M,yy}(\omega) - \alpha_{E,yy}(\omega) - \alpha_{M,xx}(\omega)]$. Upon spatio-temporal modulation, the polarizabilities adiabatically follow the harmonic driving because the response times of semiconductors are much faster than THz modulations achievable with all-optical schemes.

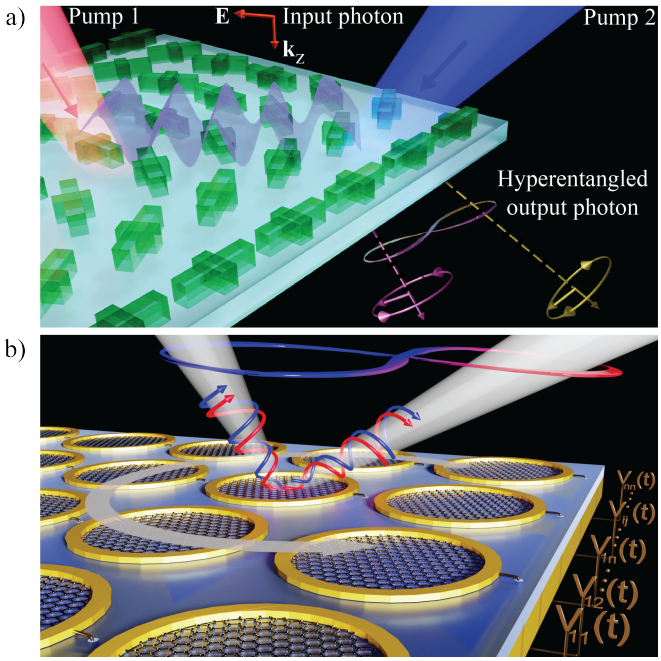

Figure 1. Conceptual representations of space-time quantum metasurfaces. (a) A dielectric STQM with refractive index modulation induces color-spin-path hyperentanglement on a single photon. (b) A graphene-disk STQM with electro-optical modulation generates entangled vortex photon pairs out of the quantum vacuum.

Hence,

$$\alpha^{(cr)}(\omega;\mathbf{r},t)=\alpha^{(cr)}_{um}(\omega)+\Delta\alpha^{(cr)}(\omega)\cos(\Omega t-\Phi(\mathbf{r})). \quad (1)$$

We calculate the polarizability modulation amplitude $\Delta\alpha^{(cr)}(\omega)$ from the dependency of $\alpha^{(cr)}_{um}(\omega)$ on permittivity modulation (Fig. 2a). The STQM Hamiltonian $H_1(t)=-\sum_{j,\gamma,\gamma'}[\alpha^{(cr)}_{um}(\omega)+\Delta\alpha^{(cr)}(\omega)\cos(\Omega t-\Phi_j)]\times A^*_{\gamma;j}A_{\gamma';j}e^{i(\omega-\omega')t}[e^{i\Psi_j}a^\dagger_{\gamma,R}a_{\gamma',L}+e^{-i\Psi_j}a^\dagger_{\gamma,L}a_{\gamma',R}]+h.c.$ results from summing contributions from individual j-th resonators. The STQM annihilates the input photon with frequency ω' and spatial mode $A_{\gamma'}$, and creates a new one with the same or Doppler-shifted frequency, flipped spin components, and added geometric and synthetic phases. Photons are very robust against decoherence in high-index dielectrics, as shown in previous experiments [5]. Temporal fluctuations in the STQM could introduce environmental noise whose quantification depends on the particular modulation protocol. For simplicity, here we consider noise-free modulations and restrict to unitary dynamics.

When the geometric phase is a linear function of the meta-atoms' positions it generates spin-path correlations, while a linear synthetic phase creates path-color correlations. The two correlations are intertwined through path and the photon evolves into a state that is hyperentangled in spin, path, and color [34]

$$|\psi(t)\rangle=\sum_{p,q}c^{(R)}_{p,q}(t)|\omega_p;\mathbf{k}_{p,q};R\rangle+c^{(L)}_{p,q}(t)|\omega_p;\mathbf{k}_{p,-q};L\rangle, \quad (2)$$

where p are integers, $q=0,1$, R (L) denotes right (left) circular polarization, $\omega_p=\omega_{in}+p\Omega$ are harmonics of the input frequency ω_{in}, $\mathbf{k}_{p,q}=\mathbf{k}_{in}+p\boldsymbol{\beta}+q\boldsymbol{\beta}_g$ are momentum harmonics of the in-plane input wave-vector $\mathbf{k}_{in}$, and $\boldsymbol{\beta}_g$ is the momentum kick induced by the geometric phase. Note the STQM makes the photon to occupy high-dimensional color qudit states. We will denote states in the first and second terms of Eq. (2) as (p,q,R) and $(p,-q,L)$, highlighting that the geometric-phase-induced momentum kicks for right- and left-polarized photons have opposite directions. To calculate the probability amplitudes we consider a normally-incident linearly-polarized single-photon pulse and assume $\Omega\ll\omega_{in}$ and $|\boldsymbol{\beta}|,|\boldsymbol{\beta}_g|\ll\omega_{in}/c$. We obtain [23]

$$|c^{(R/L)}_{p,q}(t)|^2=\frac{1}{2}\cos^2\left(\frac{\omega_{in}t\alpha^{(cr)}_{um}}{2hP^2}\right)J^2_p\left(\frac{\omega_{in}t\Delta\alpha^{(cr)}}{2hP^2}\right) \quad (3)$$

when p and q have the same parity; for opposite parity the cosine is replaced by a sine; $J_p(x)$ is the Bessel function. The probability that the output photon is in a given harmonic as a function of the modulation depth is shown in Fig. 2b. At zero modulation, the output has the same frequency as the input and is an equal superposition of right- and left-polarized geometric-phase-kicked states. As the modulation increases, transitions to only the first few frequency/momentum harmonics occur and a larger amount of the Hilbert space is explored at large modulation depths. At oblique incidence, conversion efficiencies into momentum harmonics could deteriorate due to limited performance of phase gradient metasurfaces, and wide-angle metasurfaces could be employed to enhance the transition probabilities [2]. Regarding other input polarization states, the corresponding transition probabilities are calculated in [23]. In particular, circularly-polarized input photons are cross-polarized in transmission and only get color-path entangled at the output.

Figure 2c depicts the density matrix of the input linearly-polarized photon and Figs. 2d-f the output density matrices for different configurations of the STQM: (d) Geometric phase with spatio-temporal modulation off, giving a spin-path entangled output of same frequency as input; (e) No geometric phase and spatio-temporal modulation on, resulting in multicolor-multipath entanglement; (f) Geometric phase with spatio-temporal modulation on, delivering multicolor-multipath-spin hyperentanglement.

We quantify the amount of entanglement using concurrence for qudit multi-partite systems [35, 36]. We obtain $C\approx 0.996$, $C\approx 1.129$, and $C\approx 1.381$ for Figs. 4d,e,f, respectively. Note that the concurrence in these systems is not bound to be less than one. For example, for color-path maximally entangled qudits $C_{max}=\sqrt{2}$, implying that the output state in Fig. 4e is highly entangled. Quantum state tomography or correlation measurements between different degrees of freedom of the output photon could be employed to probe entanglement. Extensions of the above analysis to other geometric and synthetic phase configurations are discussed in [23].

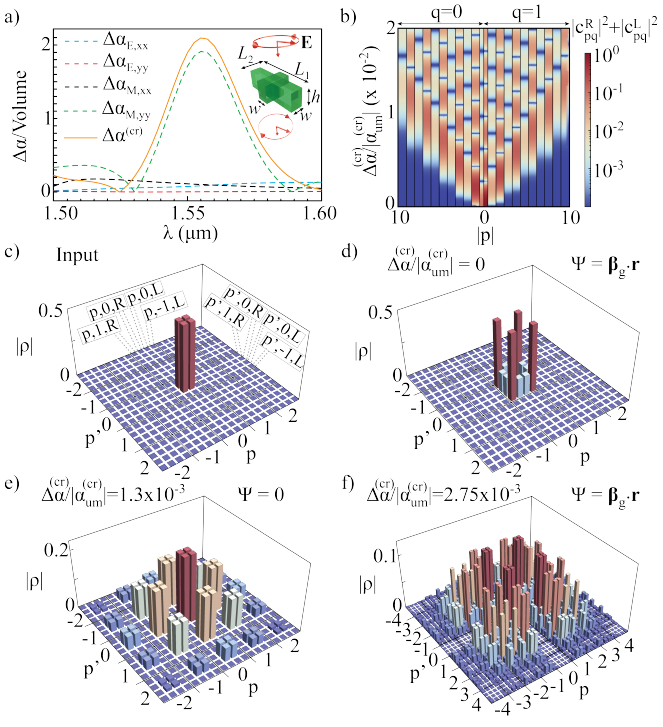

Figure 2. (a) Modulation amplitudes of polarizability tensor components normalized to the meta-atom volume for $\Delta\epsilon/\epsilon_{um} = 1\%$ of an optical all-dielectric STQM designed for maximal cross-polarized transmission at 1550 nm under normal incidence. Inset: Anisotropic amorphous Si meta-atom with $L_1 = 950$ nm, $L_2 = 435$ nm, $h = 300$ nm, $w = 200$ nm, and square unit cell with period $P = 1200$ nm. (b) Conversion probability of a linearly-polarized input photon into an output photon in frequency harmonic $\omega_{in} + p\Omega$ and momentum harmonic $p\boldsymbol{\beta}+q\boldsymbol{\beta}_g$ versus polarizability modulation depth. Density matrices of input (c) and output photons featuring (d) spin-path entanglement, (e) color-path entanglement, and (f) color-spin-path hyperentanglement. Parameters are: $\omega_{in}/2\pi = 193$ THz, $\Omega/2\pi = 10$ THz, $|\boldsymbol{\beta}| = |\boldsymbol{\beta}_g| = 0.01\omega_{in}/c$, 1 ps interaction time, and $\alpha_{um}^{(cr)} = 0.6\mu\text{m}^3$ [23].

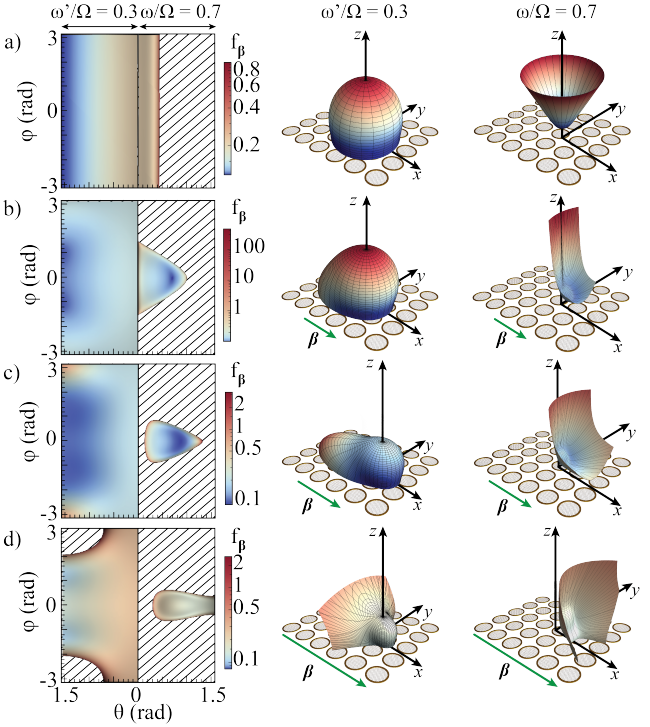

Figure 3. Steered quantum vacuum from a graphene-disk STQM. Density (first column) polar plots of emitted circularly-polarized radiation for various momentum kicks $c\beta/\Omega$ equal to 0 (a), 0.3 (b), 0.38 (c), and 0.5 (d). The areas to the right (left) of the vertical solid line correspond to the emission spectrum of the high- (low-) frequency photon in a pair. The second and third columns show the corresponding spherical polar plots. Parameters are: $\Omega/2\pi = 10$ THz, $\Delta E_F/E_F = 1\%$, $n_{MS} = 10^3$ mm^{-2}, $D = 5$ μm, and $\mu = 10^4$ cm^2 V^{-1} s^{-1}.

STQM-enabled quantum vacuum manipulation: We now study STQMs comprising modulated quantum materials [37] and manipulating quantum vacuum fluctuations. As a simple example, we consider a graphene-disk STQM whose Fermi energy E_F is spatio-temporally modulated, $E_F(\mathbf{r},t) = E_F + \Delta E_F \cos(\Omega t - \Phi(\mathbf{r}))$. The geometric phase is zero and, in the intraband regime, the modulation of E_F results in a corresponding modulation of the electric polarizability of the disks, $\alpha(\omega;\mathbf{r},t) = \alpha_{um}(\omega) + \Delta\alpha(\omega)\cos(\Omega t - \Phi(\mathbf{r}))$. The highly localized plasmons supported by the graphene disks [38–40] result in resonant enhancements of $\Delta\alpha(\omega)$ conducive to efficient coupling of the STQM with the quantum vacuum (inset Fig. 4e). Furthermore, the use of ultra-high mobility graphene minimizes photon absorption [41, 42], which is also desired feature for enhancing the coupling. We design the metasurface to operate in the low-THz regime, and consider modulation frequencies also in the same range, which can be achieved using dynamic optical gratings and graphene's Kerr nonlinearity [23].

The STQM couples to the quantum electromagnetic field via the photon-number-non-conserving Hamiltonian $H_2(t) = (1/8)\sum_{j,\gamma,\gamma'}\sum_{\lambda,\lambda'} [\Delta\alpha(\omega) + \Delta\alpha(\omega')] \times A^*_{\gamma;j}A^*_{\gamma';j}\, e^{i\Phi_j} e^{i(\omega+\omega'-\Omega)t}\, a^\dagger_{\gamma,\lambda}a^\dagger_{\gamma',\lambda'} + h.c.$, where λ, λ' are polarization states of the two photons. This process is essentially an analogue of the dynamical Casimir effect (DCE) in which an oscillating boundary parametrically excites virtual into real photons [43–45]. Interestingly, the STQM synthetic phase allows for a novel degree of control over the quantum vacuum, beyond previously demonstrated analog DCE set-ups [46–49]. Indeed, steered and twisted DCE photons can be produced and the DCE scattering matrix becomes asymmetric [50], reflecting that Lorentz reciprocity is broken at the level of quantum vacuum fluctuations [51].

We compute the rates of photon production out of the quantum vacuum using time-dependent perturbation theory by assuming weak modulation depths of the meta-atoms (other possible approaches are discussed in [44, 45]). Energy conservation dictates that the photon pairs satisfy $\omega + \omega' = \Omega$. The two-photon emission rate from an STQM of area A with arbi-

trary synthetic phase $\Phi(\mathbf{r})$ is

$$\Gamma_\Phi = \frac{An_{MS}^2\Omega^4}{512\pi^3c^4}\int_0^\Omega d\omega|\Delta\alpha(\omega)+\Delta\alpha(\Omega-\omega)|^2 f_\Phi(\omega). \quad (4)$$

The rate scales as the square of the meta-atoms number surface density n_{MS}, indicating coherent emission of photon pairs. The spectral weight function $f_\Phi(\omega)$ results from the integration of all two-photon generation events encoded in the angular emission spectrum. In Figure 3 we show this spectrum $f_\beta(\mathbf{k},\omega)$ for the case of the linear synthetic phase. Momentum conservation enforces that the emitted photons must have in-plane momenta that add up to the imprinted kick, $\mathbf{k}+\mathbf{k}'=\boldsymbol{\beta}$, and the emitted photons are entangled over continuous colors and paths. In the absence of kick the spectra resemble cone- (dome-) like shapes for the high- (low-) frequency photon. As the magnitude of the momentum kick β increases, the emission profiles undergo intricate changes. The directions of allowed emission for the first (second) photon get deformed until at $\beta_{max}=\Omega/c$ they collapse to a single direction and the photon is only emitted parallel (anti-parallel) to the kick. The modulation also excites hybrid entangled pairs composed of one photon and one evanescent surface wave (shaded areas in the left panels), and when $\beta>\beta_{max}$ only evanescent modes are created. The spectral weight function $f_\beta(\omega)$ is plotted in Fig. 4a. At zero kick it has a singular behavior at $\omega/\Omega=0.5$ which results from events where both photons are emitted at grazing angles [52]. For nonzero kick the modulation induces an asymmetry between the photons and such singular events cannot take place. The spectrum develops a central plateau-like form with sharp edges at $\omega_\pm/\Omega=(1\pm c\beta/\Omega)/2$, corresponding to cases where the high (low) frequency photon starts (stops) to be emitted at grazing angles and in azimuthal directions parallel (antiparallel) to the kick.

The STQM can also stir the quantum vacuum and induce angular momentum nonreciprocity [53] that results in entangled vortex-pair generation (Fig. 1b). The required synthetic phase to induce such a process is the spinning phase $\Phi(\mathbf{r})=\ell\varphi$ (ℓ is an arbitrary integer and φ is the azimuthal angle). The modulated metasurface generates photon pairs carrying angular momenta that add up to the imprinted spinning $m+m'=\ell$ in agreement with angular momentum conservation. Photons are color-angular momentum entangled and their correlations could be probed using photo-coincidence detection and techniques based on angular momentum sorting of light [54, 55]. The spectral weight function $f_\ell(\omega)$ is reported in Fig. 4b, showing plateau-like structures with decreasing height as the spinning grows. There is a drastic but subtle difference between $f_\beta(\omega)$ and $f_\ell(\omega)$ that is not apparent in the plots: The former vanishes beyond the finite kick threshold β_{max}, while there is no finite spinning threshold for the latter. Figures 4c-d show the angular momentum spectra of low- and high-frequency photons in an emitted pair. Due to color-angular momentum entanglement and the conservations laws derived above, the probability of emitting a photon with (ω,m) must be the identical to that of creating a photon with $(\Omega-\omega,\ell-m)$. When the STQM does not imprint

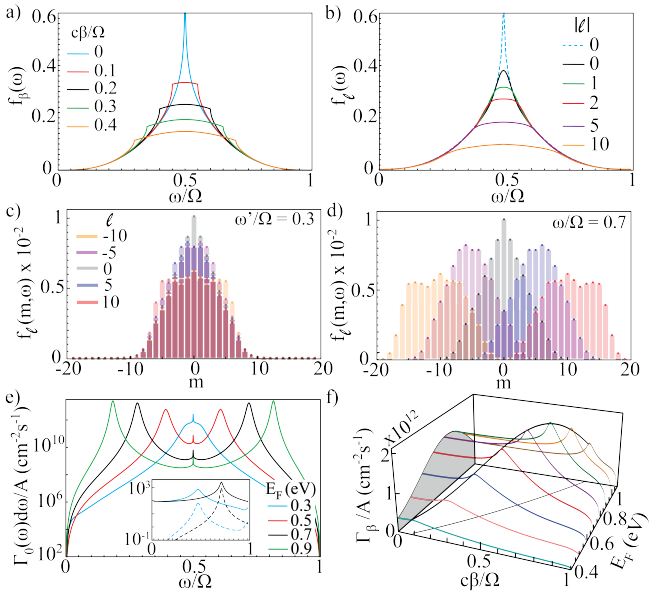

Figure 4. Spectral weight function for (a) linear and (b) rotating synthetic phase. Solid lines in (b) correspond to a finite radius metasurface ($\Omega R/c=30$) and dashed line is the $\ell=0$ case for an infinite metasurface. Angular-momentum spectra for finite radius metasurface for the (c) low- and (d) high-frequency photon. (e) Spectral photo-production rate for null synthetic phase for a graphene-disk STQM. Inset: unmodulated electric polarizability $\alpha_{um}(\omega)$ (solid) and modulation amplitude $\Delta\alpha(\omega)$ (dashed) in units of μm^3. (f) Emission rate for linear synthetic phase. The black thick curve joins peaks of maximal emission and the thin black curve $\omega_{res}(E_F)=(\Omega+c\beta)/2$ is its projection on the $\beta-E_F$ plane. Parameters are the same as in Fig. 3.

any spinning, the spectra are symmetric around the peak at $m=0$, with oppositely twisted photons in each emitted pair. When spinning is present, one intuitively expects that photons will be emitted with the same angular momentum as the drive ($m=\ell$), and because they are created in pairs with complementary angular momentum, emission at $m=0$ should be equally probable, as verified in Figs. 4c,d.

Figure 4e depicts the spectral rate for a STQM for null synthetic phase, featuring Lorentzian peaks at complementary frequencies. For high-Q resonances the emission rate for arbitrary synthetic phase is approximated as

$$\Gamma_\Phi \approx g\Omega\,(An_{MS}^2D^6\omega_{res}^4/c^4)\,f_{\Phi;res}\Big(\frac{\Delta E_F}{E_F}\Big)^2\Big(\frac{\Omega}{\gamma}\Big)^3. \quad (5)$$

Here, $\omega_{res}=(e^2E_F/4\pi^2\varepsilon_0|\xi_1|\hbar^2D)^{1/2}$ is the resonance frequency, D the disk diameter, $f_{\Phi;res}$ the spectral weight on resonance, $\gamma=ev_F^2/E_F\mu$ (Fermi velocity v_F and mobility μ), and $g=5\pi^4a_1^4\xi_1^2/2(512)^3$ is determined by the lowest plasmonic eigenmode coefficients $a_1=6.1$ and $\xi_1=-0.072$. Figure 4f shows the emission rate for the linear synthetic phase as a function of momentum kick and Fermi energy. Giant photon-pair production rates on the order of 10^{12} photons/cm^{2}s are obtained at low-THz driving frequencies and modest modulation depths.

In conclusion, we uncovered a key property of space-time quantum metasurfaces relevant for potential applications: On-demand reconfiguration of the synthetic phase allows dynamically tunable quantum correlations, enabling to tailor the nature of entanglement depending on the symmetry properties of both geometric and synthetic phases. We also illustrated a second key property of space-time quantum metasurfaces with fundamental relevance: Lorentz nonreciprocity at the deepest level of vacuum fluctuations is attained through joint space and time modulations of optical properties and can be interpreted as an asymmetric quantum vacuum. Novel photonic devices potentially enabled by the proposed STQM concept include quantum emitters with reconfigurable spatial modes, quantum nonreciprocal routers and isolators for free-space photon transport in distributed quantum networks, and active quantum sensors with photon steering capabilities to scan a detection area of interest. Beyond solid-state quantum metasurfaces, the extension of the proposed STQM concept to atomic-scale quantum metasurfaces, such as two-dimensional atomic arrays in an optical lattice, could open new paths for manipulating cooperative light-matter interactions at the single-quantum level. As such, space-time quantum metasurfaces can provide breakthrough advances in the broad field of quantum science and technology.

This work was supported by the DARPA QUEST and LANL LDRD programs. We are grateful to A. Efimov, M. Julian, C. Lewis, M. Lucero, and A. Manjavacas for discussions.

*Correspondence: dalvit@lanl.gov

[1] A. V. Kildishev, A. Boltasseva, and V. M. Shalaev, Planar photonics with metasurfaces, Science **339**, 1232009 (2013).

[2] H.-T. Chen, A. J. Taylor, and N. Yu, A review of metasurfaces: physics and applications, Rep. Prog. Phys. **79**, 076401 (2016).

[3] P. K. Jha, X. Ni, C. Wu, Y. Wang, and X. Zhang, Metasurface-Enabled Remote Quantum Interference, Phys. Rev. Lett. **115**, 025501 (2015).

[4] A. S. Solntsev, G. S. Agarwal, and Y. S. Kivshar, Metasurfaces for quantum photonics, arXiv:2007.14722.

[5] T. Stav, A. Faerman, E. Maguid, D. Oren, V. Kleiner, E. Hasman, and M. Segev, Quantum entanglement of the spin and orbital angular momentum of photons using metamaterials, Science **361**, 1101-1104 (2018).

[6] P. K. Jha, N. Shitrit, J. Kim, X.Ren, Y. Wang, and X. Zhang, Metasurface-Mediated Quantum Entanglement, ACS Photonics **5**, 971-976 (2018).

[7] K. Wang, J. G. Titchener, S. S. Kruk, L. Xu, H.-P. Chung, M. Parry, I. I. Kravchenko, Y.-H. Chen, A. S. Solntsev, Y. S. Kivshar, D. N. Neshev, and A. A. Sukhorukov, Quantum metasurface for multiphoton interference and state reconstruction, Science **361**, 1104-1108 (2018).

[8] P. Georgi, M. Massaro, K.-H. Luo, B. Sain, N, Montaut, H. Herrmann, T. Weiss, G. Li, C. Silberhorn, and T. Zentgraf, Metasurface interferometry toward quantum sensors, Light: Science & Applications **8**, 70 (2019).

[9] J. Bohn, T. Bucher, K. E. Chong, A. Komar, D.-Y. Choi, D. N. Neshev, Y. S. Kivshar, T. Pertsch, and I. Staude, Active tuning of spontaneous emission by Mie-resonant dielectric metasurfaces, Nano Lett. **18**, 3461-3465 (2018).

[10] A. Vaskin, R. Kolkowskia, A. F. Koenderink, and I. Staude, Light-emitting metasurfaces, Nanophotonics **8**, 1151-1198 (2019).

[11] Y.-Y. Xie, P.-N. Ni, Q.-H. Wang, Q. Kan, G. Briere, P.-P. Chen, Z.-Z. Zhao, A. Delga, H.-R. Ren, H.-D. Chen, C. Xu, and P. Genevet, Metasurface-integrated vertical cavity surface-emitting lasers for programmable directional lasing emissions, Nat. Nanotech. **15**, 1250-130 (2020).

[12] Y. Kan, S. K. H. Andersen, F. Ding, S. Kumar, C. Zhao, and S. I. Bozhevolnyi, Metasurface-enabled generation of circularly polarized single photons, Adv. Mater. **32**, 1907832 (2020).

[13] L. Li, Z. Liu, X. Ren, S. Wang, V. Su, M.-K. Chen, C. H. Chu, H. Y. Kuo, Bi. Liu, W. Zang, G. Guo, L. Zhang, Z. Wang, S. Zhu, and D. P. Tsai, Metalens-array-based high-dimensional and multiphoton quantum source, Science **368**, 1487-1490 (2020).

[14] Q. Li, W. Bao, Z. Nie, Y. Xia, Y. Xue, Y.Wang, S. Yang, and X. Zhang, A non-unitary metasurface enables continuous control of quantum photon-photon interactions from bosonic to fermionic, Nat. Photonics **15**, 267-271 (2021).

[15] R. Bekenstein, I. Pikovski, H. Pichler, E. Shahmoon, S. F. Yelin, and M. D. Lukin, Quantum metasurfaces with atom arrays, Nat. Phys. **16**, 676-681 (2020).

[16] J. Rui, D. Wei, A. Rubio-Abadal, S. Hollerith, J. Zeiher, D. M. Stamper-Kurn, C. Gross, and I. Bloch, A subradiant optical mirror formed by a single structured atomic layer, Nature **583**, 369-374 (2020).

[17] A. M. Shaltout, V. M. Shalaev, and M. L. Brongersma, Spatiotemporal light control with active metasurfaces, Science **364**, 648 (2019).

[18] C. Caloz and Z.-L. Deck-Léger, Spacetime Metamaterials, IEEE Transactions on Antennas and Propagation **68**, 1569-1582 (2019).

[19] A. E. Cardin, S. R. Silva, S. R. Vardeny, W. J. Padilla, A. Saxena, A. J. Taylor, W. J. M. Kort-Kamp, H.-T. Chen, D. A. R. Dalvit, and A. K. Azad, Surface-wave-assisted nonreciprocity in spatio-temporally modulated metasurfaces, Nat. Commun. **11**, 1469 (2020).

[20] L. Zhang, X. Q. Chen, S. Liu, Q. Zhang, J. Zhao, J. Y. Dai, G. D. Bai, X. Wan, Q. Cheng, G. Castaldi, V. Galdi, and T. J. Cui, Space-time-coding digital metasurfaces, Nat. Commun. **9**, 4334 (2018).

[21] Z. Bomzon, G. Biener, V. Kleiner, and E. Hasman, Space-variant Pancharatnam-Berry phase optical elements with computer-generated subwavelength gratings, Opt. Lett. **27**, 1141-1143 (2002).

[22] X. Guo, Y. Ding, Y. Duan, and X. Ni, Nonreciprocal metasurface with space-time phase modulation, Light: Science & Applications **8**, 123 (2019).

[23] See Supplementary Information, that contains references [24–31].

[24] A. B. Evlyukhin, C. Reinhardt, E. Evlyukhin, and B. N. Chichkov, Multipole analysis of light scattering by arbitrary-shaped nanoparticles on a plane surface, J. Opt. Soc. Am. B **30**, 2589 (2013).

[25] H. J. Eichler, P. Günter, and D. H. Pohl, *Laser induced dynamical gratings* (Springer-Verlag, Heidelberg, 1986).

[26] D. Naidoo, K. Ait-Ameur, M. Brunel, and A. Forbes, Intracavity generation of superpositions of Laguerre-Gaussian beams, Appl. Phys. B, **106**, 683-690 (2012).

[27] G. F. Calvo, A. Picón, and E. Bagan, Quantum field theory of photons with orbital angular momentum, Phys. Rev. A **73**, 013805 (2006).

[28] J. L. Cheng, N. Vermeulen and J. E. Sipe, Third-order nonlinearity of graphene: Effects of phenomenological relaxation and finite temperature, Phys. Rev. B **91**, 235320 (2015).

[29] S. A. Mikhailov, Quantum theory of the third-order nonlinear electrodynamic effects of graphene, Phys. Rev. B **93**, 085403 (2016).

[30] C. L. Holloway, M. A. Mohamed, E. F. Kuester, and A. Dienstfrey, Reflection and transmission properties of a metafilm: with an application to a controllable surface composed of resonant particles, IEEE Transactions on Electromagnetic Compatibility **47**, 853-865 (2005).

[31] S. J. Van Enk and G. Nienhuis, Commutation rules and eigenvalues of spin and orbital angular momentum of radiation fields, J. Mod. Opt. **41**, 963-977 (1994).

[32] A. I. Kuznetsov, A. E. Miroshnichenko, M. L. Brongersma, Y. S Kivshar, and B. Luk'yanchuk, Optically resonant dielectric nanostructures, Science **354**, aag2472 (2016).

[33] L. Novotny and B. Hecht, *Principles of Nano-Optics* (Cambridge University Press, New York, 2007).

[34] J. T. Barreiro, N. K. Langford, N. A. Peters, and P. G. Kwiat, Generation of Hyperentangled Photons Pairs, Phys. Rev. Lett. **95**, 260501 (2005).

[35] P. Rungta, V. Buzek, C. M. Caves, M. Hillery, and G. J. Milburn, Universal state inversion and concurrence in arbitrary dimensions, Phys. Rev. A **64**, 042315 (2001).

[36] F. Mintert, A. R. R. Carvalho, M. KuÅ>, and A. Buchleitner, Measures and dynamics of entangled states, Phys. Reports **415**, 207-259 (2005).

[37] B. Keimer and J. E. Moore, The physics of quantum materials, Nat. Phys. **13**, 1045-1055 (2017).

[38] R. Yu, J. D. Cox, J. R. M. Saavedra, and F. J. García de Abajo, Analytical modeling of graphene plasmons, ACS Photonics **4**, 3106 (2017).

[39] F. J. García de Abajo and A. Manjavacas, Plasmonics in atomically thin materials, Faraday Discuss. **178**, 87-1073548 (2015).

[40] Y. Muniz, A. Manjavacas, C. Farina, D. A. R. Dalvit, and W. J. M. Kort-Kamp, Two-Photon Spontaneous Emission in Atomically Thin Plasmonic Nanostructures, Phys. Rev. Lett. **125**, 033601 (2020).

[41] K. I. Bolotin, K. J. Sikes, Z. Jiang, M. Klima, G. Fudenberg, J. Hone, P. Kim, and H. L. Stormer, Ultrahigh electron mobility in suspended graphene, Solid State Commun. **146**, 351-355 (2008).

[42] C. R. Dean, A. F. Young, I. Meric, C. Lee, L. Wang, S. Sorgenfrei, K. Watanabe, T. Taniguchi, P. Kim, K. L. Shepard, and J. Hone, Boron nitride substrates for high-quality graphene electronics, Nat. Nanotechnol. **5**, 722-726 (2010).

[43] G. T. Moore, Quantum theory of the electromagnetic field in a variable-length one-dimensional cavity, Journal of Mathematical Physics **11**, 2679 (1970).

[44] D. A. R. Dalvit, P. A. Maia Neto, and F. D. Mazzitelli, in Casimir Physics, Lecture Notes in Physics **834** (eds. D. Dalvit, P. Milonni, D. Roberts, and F. Da Rosa), (Springer, Heidelberg, 2006).

[45] V. V. Dodonov, Current status of the dynamical Casimir effect, Physica Scripta **82**, 038105 (2010).

[46] C. M. Wilson, G. Johansson, A. Pourkabirian, M. Simoen, J. R. Johansson, T. Duty, F. Nori, and P. Delsing, Observation of the dynamical Casimir effect in a superconducting circuit, Nature **479**, 376-379 (2011).

[47] J.-C. Jaskula, G. B. Partridge, M. Bonneau, R. Lopes, J. Ruaudel, D. Boiron, and C. I. Westbrook, Acoustic Analog to the Dynamical Casimir Effect in a Bose-Einstein Condensate, Phys. Rev. Lett. **109**, 220401 (2012).

[48] P. Lahteenmaki, G. S. Paraoanu, J. Hassel, and P. J. Hakonen, Dynamical Casimir effect in a Josephson metamaterial, Proc. Nat. Acad. Sci. USA **110**, 4234-4238 (2013).

[49] S. Vezzoli, A. Mussot, N. Westerberg, A. Kudlinski, H. D. Saleh, A. Prain, F. Biancalana, E. Lantz, and D. Faccio, Optical analogue of the dynamical Casimir effect in a dispersion-oscillating fibre, Commun. Phys. **2**, 84 (2019).

[50] M. F. Maghrebi, R. Golestanian, and M. Kardar, Scattering approach to the dynamical Casimir effect, Phys. Rev. D **87**, 025016 (2013).

[51] D. L. Sounas and A. Alù, Non-reciprocal photonics based on time modulation, Nat. Photonics **1**, 774-783 (2017).

[52] P. A. Maia Neto and L. A. S. Machado, Quantum radiation generated by a moving mirror in free space, Phys. Rev. A **54**, 3420 (1996).

[53] D. L. Sounas, C. Caloz, and A. Alù, Giant non-reciprocity at the subwavelength scale using angular momentum-biased metamaterials, Nat. Commun. **4**, 2407 (2013).

[54] G. C. Berkhout, M. P. Lavery, J. Courtial, M. W. Beijersbergen, and M. J. Padgett, Efficient Sorting of Orbital Angular Momentum States of Light, Phys. Rev. Lett. **105**, 153601 (2010).

[55] M. Mirhosseini, M. Malik, Z. Shi, and R. W. Boyd, Efficient separation of the orbital angular momentum eigenstates of light, Nat. Commun. **4**, 2783 (2013).